Bioinformatics-based identification of GH12 endoxyloglucanases in citrus-pathogenic Penicillium spp

Li, Kai; Barrett, Kristian; Agger, Jane W.; Zeuner, Birgitte; Meyer, Anne S.

Published in:
Enzyme and Microbial Technology

Link to article, DOI:
10.1016/j.enzmictec.2024.110441

Publication date:
2024

Document Version
Publisher's PDF, also known as Version of record

Enzyme and Microbial Technology 178 (2024) 110441

Contents lists available at ScienceDirect

Enzyme and Microbial Technology

journal homepage: www.elsevier.com/locate/enzmictec

Bioinformatics-based identification of GH12 endoxyloglucanases in citrus-pathogenic *Penicillium* spp

Kai Li [1], Kristian Barrett, Jane W. Agger, Birgitte Zeuner [*], Anne S. Meyer

Department of Biotechnology and Biomedicine, Technical University of Denmark, Søltofts Plads 221, Kgs. Lyngby 2800, Denmark

ARTICLE INFO

Keywords:
Citrus peel xyloglucan
Endoxyloglucanase
GH12
LC-MS
Penicillium spp

ABSTRACT

Millions of tons of citrus peel waste are produced every year as a byproduct of the juice industry. Citrus peel is rich in pectin and xyloglucan, but while the pectin is extracted for use in the food industry, the xyloglucan is currently not valorized. To target hydrolytic degradation of citrus peel xyloglucan into oligosaccharides, we have used bioinformatics to identify three glycoside hydrolase 12 (GH12) endoxyloglucanases (EC 3.2.1.151) from the citrus fruit pathogens *Penicillium italicum* GL-Gan1 and *Penicillium digitatum* Pd1 and characterized them on xyloglucan obtained by alkaline extraction from citrus peel. The enzymes displayed pH-temperature optima of pH 4.6–5.3 and 35–37°C. PdGH12 from *P. digitatum* and PiGH12A from *P. italicum* share 84% sequence identity and displayed similar kinetics, although k_{cat} was highest for PdGH12. In contrast, PiGH12B from *P. italicum*, which has the otherwise conserved Trp in subsite −4 replaced with a Tyr, displayed a 3 times higher K_M and a 4 times lower k_{cat}/K_M than PiGH12A, but was the most thermostable enzyme of the three *Penicillium*-derived endoxyloglucanases. The benchmark enzyme AnGH12 from *Aspergillus nidulans* was more thermally stable and had a higher pH-temperature optimum than the enzymes from *Penicillum* spp. The difference in structure of the xyloglucan oligosaccharides extracted from citrus peel xyloglucan and tamarind xyloglucan by the new endoxyloglucanases was determined by LC-MS. The inclusion of citrus peel xyloglucan demonstrated that the endoxyloglucanases liberated fucosylated xyloglucan oligomers, implying that these enzymes have the potential to upgrade citrus peel residues to produce oligomers useful as intermediates or bioactive compounds.

1. Introduction

The citrus fruits, which include orange, tangerine, lemon, lime and grapefruit, are regarded as major agricultural raw materials in the fruit juice industry. In 2020, the annual global production was over 140 million tons, of which more than 20 million tons were processed for juice production [1]. The citrus peel is mainly used for pectin and citrus oil extraction, but even after this valorization, more than 80% of the peel remains as a low value residue [2]. As a result, the further upcycling of citrus peel waste is currently receiving more attention. As fruit industry residues such as citrus peel and apple pomace are rich in both pectin and xyloglucan, the subsequent extraction target for the side streams that remain after pectin extraction is often xyloglucan [2,3]. Evidence is mounting that xyloglucan and xyloglucan oligosaccharides can function as prebiotics [4,5], and recently a study demonstrated that tamarind xyloglucan oligosaccharides could attenuate metabolic disorders [6]. Previously, we have extracted xyloglucan from citrus peel by alkaline treatment to valorize its fucose content via enzymatic transglycosylation synthesis of fucosylated human milk oligosaccharides [7,8]. The degree of xyloglucan fucosylation is highly dependent on the plant source; while seed xyloglucan such as that from tamarind has no fucose, xyloglucan from citrus peel contains fucogalactoxylo side chains with a terminal α-1,2-linked fucose [2,9–11]. Importantly, the yield of fucosylated products from the enzymatic transglycosylation increased when the extracted citrus peel was depolymerized by an endoxyloglucanase [12]. Further, it was recently demonstrated that enzymatic extraction of xyloglucan from depectinized lemon and orange peel preserved more fucose and gave rise to higher transglycosylation yields than the alkaline extraction [2].

Endoxyloglucanases can catalyze hydrolysis of the backbone of xyloglucans, and can thus play an important role in the production of xyloglucan oligosaccharides. In the CAZy database of glycoside hydrolase (GH) families, endoxyloglucanases are classified in GH5, GH9, GH12, GH16, GH44, GH45, and GH74 families, with the majority

* Corresponding author.
E-mail address: bzeu@dtu.dk (B. Zeuner).
[1] Present address: College of Chemical and Biological Engineering, Shandong University of Science and Technology, Qingdao 266590, China

https://doi.org/10.1016/j.enzmictec.2024.110441
Received 21 December 2023; Received in revised form 25 March 2024; Accepted 26 March 2024
Available online 29 March 2024

belonging to either GH12 or GH74 [13]. Neither of these families are isofunctional, and the enzymes in GH12, which are all endo-β-glucanases, can be classified into three different activities: endo-β-1,4-glucanase (EC 3.2.1.4), endoxyloglucanase (EC 3.2.1.151), and β-1,3–1,4-glucanase (EC 3.2.1.73). Thus, the most important xyloglucan-specific hydrolases in GH12 are the endoxyloglucanases, also known as xyloglucan-specific endo-β-1,4-glucanases (EC 3.2.1.151) with a retaining reaction mechanism that hydrolyze the backbone linkage on the reducing end side of unbranched glucose residues in xyloglucan [13,14]. Numerous GH12 endoxyloglucanases have been characterized from *Aspergillus* species, including those of *Aspergillus aculeatus* [15], *Aspergillus cervinus* [16], *Aspergillus clavatus* [17], *Aspergillus fumigatus* [18,19], *Aspergillus niger* [20], *Aspergillus niveus* [21], *Aspergillus nidulans* [22], *Aspergillus oryzae* [23], and *Aspergillus terreus* [24]. The xyloglucan-degrading enzyme machinery of *Aspergillus* species was recently reviewed [25]. In comparison, there is room for more discoveries outside the Aspergilli. Only a few GH12 endoxyloglucanases have been characterized from *Penicillum* species, namely those from *Penicillum oxalicum* [26,27], *Penicillum verruculosum* and *Penicillum canescens* [28]. Other characterized fungal GH12 include two endoxyloglucanases from *Rhizomucor miehei* [29], and one from each of the plant pathogens *Phytophtora sojae* [30], *Fusarium graminearum* [31], and *Pyricularia oryzae* [32]. Finally, two bacterial GH12 endoxyloglucanases have been characterized from *Bacillus licheniformis* [33] and from *Sinorhizobium fredii* [34].

It has been observed that filamentous fungi whose habitat include a wide host range, i.e. a wide range of biomass they can live on, have a larger genome than those with a narrower host range [35]. An example of a filamentous fungus with a comparatively small genome is *Penicillium sclerotigenum*, which is a pathogen of certain tubers that belongs to the same taxonomical section (*Penicillium*) as *Penicillum italicum* and *Penicillum digitatum*; this section harbors pathogens of pectin- and xyloglucan-rich crops such as apples and citrus fruits [35,36]. The proteome and transcriptome of *P. sclerotigenum* was recently elucidated when the strain was grown on sweet potato pectin, and the conserved unique peptide pattern (CUPP) bioinformatic tool was applied to infer substrate specificity [36]. The CUPP online server, cupp.info, is widely applicable for functional prediction of enzyme specificities [37–39], and was recently applied to map substrate specificity of α-L-fucosidases across the GH29 family [40].

With the objective of specifically targeting citrus peel valorization, we here describe the discovery, recombinant expression in *Pichia pastoris* X-33, and characterization of three novel GH12 endoxyloglucanases from *Penicillium* spp. known to be citrus fruit pathogens. A key objective was to find xyloglucan-degrading enzymes active on fucosylated citrus peel xyloglucan. The hydrolytic activity, pH-temperature optima, and kinetic parameters of the enzymes are determined, and we investigate the active site structure in homology models. A well-characterized GH12 endoxyloglucanase from *A. nidulans* was included for comparison [22,41]. Finally, we performed liquid chromatography-mass spectrometry (LC-MS) analysis to elucidate the product formation of the xyloglucan oligomers released by the *Penicillum* derived endoxyloglucanases from citrus peel xyloglucan as compared to those released from the benchmark tamarind xyloglucan.

2. Materials and methods

2.1. Chemicals

Dried citrus peel was provided by Dupont Nutrition BioSciences ApS (Brabrand, Denmark), which was used to extract the xyloglucan. The citrus peel was grounded using a MF 10 basic mill (IKA-Werke GmbH & Co. KG, Staufen, Germany) and then stored at −20 °C until alkaline extraction. The tamarind xyloglucan and xyloglucan standards (XXXG, XXLG, XXFG and XLLG) were purchased from Megazyme (Wicklow, Ireland). All the chemicals used were analytical grade.

2.2. Alkaline extraction for citrus peel xyloglucan

The citrus peel xyloglucan was produced by alkaline extraction as described previously [7]. Citrus peel powder (20 g) was suspended in 1 L of 24% (*w/v*) potassium hydroxide with 0.1% (*w/v*) sodium borohydride during 24 h magnetic stirring at room temperature. Afterwards, the suspension was neutralized with acetic acid and then centrifuged at 5000 g for 30 minutes. The supernatant was filtered sequentially with filter paper and 0.22 μm filter to remove large and small insoluble particles. After adding a lot of MilliQ water, the supernatant was dialysed using a 5 kDa Vivaflow 200 membrane (Sartorius, Göttingen, Germany) to remove salts and low molecular weight molecules (such as monosaccharides). Lastly, the retentate after dialysis was freeze-dried and stored at 4 °C until use. The monosaccharide composition and molecular weight distribution of citrus peel xyloglucan was determined by a previous study [7].

2.3. Enzyme selection, expression and purification

The strains *P. digitatum* Pd1 and *P. italicum* GL-Gan1 were selected for GH12 discovery [35]. The full genome of *P. italicum* GL-Gan1 was downloaded from NCBI (GCA_002116305.1). The encoding genes and corresponding proteins were predicted using Augustus 2.5 (http://bioinf.uni-greifswald.de/augustus/) with model *A. oryzae* [35,42], whereas the protein list available from NCBI was used for *P. digitatum* Pd1. Functional annotation was performed by the Conserved Unique Peptide Patterns (CUPP) webserver at cupp.info [37,38]. CUPP analysis of the entire GH12 family was performed by downloading the annotations from cupp.info and visualizing them in iTOL [43]. From this, all GH12s from these two strains predicted to be endoxyloglucanases (EC 3.2.1.151) were selected for expression: PdGH12 from *P. digitatum* Pd1 (GenBank EKV19943.1), PiGH12A and PiGH12B from *P. italicum* GL-Gan1 (Table S2). The signal peptides for three endoxyloglucanases were predicted by SignalP 5.0 [44]. All the signal peptide sequences were removed from the sequence, and the resulting sequences (Table S2) were codon-optimized and inserted into the pPICZα-A expression vector with a C-terminal His_6-tag sequence for expression in *P. pastoris* by GenScript (Leiden, Netherlands). The plasmids were transformed into competent *E. coli* DH5α for plasmid propagation. After plasmid extraction, the plasmids were linearized with restriction enzyme (*MssI*) for 6 hours at 37 °C, desalted, and kept at −20 °C for *P. pastoris* transformation.

The genes for PdGH12, PiGH12A and PiGH12B, were expressed in *P. pastoris* X-33 and the resulting enzymes were purified as described previously [45]. In general, *P. pastoris* X-33 was transformed with the linearized plasmid by electroporation and selected for Zeocin resistance. The transformants were grown for 24 hours in buffered glycerol complex medium (BMGY) with Zeocin at 30°C. The cultures were harvested by centrifugation (2500 *g*, 15 min) and the pellet was resuspended in buffered methanol complex medium (BMMY) to an OD_{600} of 1. The cells were grown for 72 hours at 28 °C and the production was induced by methanol (0.5% *v/v*) every 24 hours. After the expression, the cultures were harvested by centrifugation (5000 *g*, 25 min and 4 °C), and then the supernatant was collected and concentrated on a 10 kDa Vivaspin 20 column (Sartorius, Göttingen, Germany). As described previously [46], the concentrated supernatant was filtered through a 0.45 μm filter and then purified using a gravity flow type of Ni^{2+} affinity chromatography with 20 mM sodium acetate buffer pH 6.0, 20 mM imidazole and 100 mM sodium chloride as binding buffer and 20 mM sodium acetate buffer pH 6.0, 500 mM imidazole and 100 mM sodium chloride as elution buffer. The purified enzyme was desalted using PD-10 columns (GE Healthcare, Uppsala, Sweden) and using the imidazole-free exchange buffer (20 mM acetate buffer pH 6.0 with 100 mM sodium chloride). The benchmark enzyme AnGH12 (AN0452.2; GenBank accession no. EAA66551.1) from *A. nidulans* [47]. was produced in a 5 L fermentor in *P. pastoris* X-33 as described previously [45]. The

purification and desalting processes were carried out as above. The enzyme purity was confirmed by SDS-PAGE and the enzyme concentration was measured by the ROTI®-Nanoquant assay (The Carl Roth GmbH + Co. KG, Karlsruhe, Germany), which is a modification of the Bradford assay, using bovine serum albumin (BSA) standards.

2.4. Optimal pH and temperature conditions

The optimum pH-temperature conditions were determined by response surface methodology (RSM) with two factors and three levels of factorial design using citrus peel xyloglucan as substrate; the use of RSM can capture the temperature dependence of the pH optimum. All reaction conditions were selected based on preliminary experiments to achieve optimal reaction time, substrate and enzyme concentrations, and ranges of pH and temperature. The substrate was dissolved in 50 mM sodium acetate buffer, and the citrus peel xyloglucan concentration was 40 g L^{-1} in the reaction. All the reactions were performed with an enzyme-to-substrate ratio (E/S) of 0.004% (*w/w*), and two different reaction times were used in this experiment: 30 minutes (AnGH12) and 1 hour (PdGH12, PiGH12A and PiGH12B). For PdGH12, PiGH12A and PiGH12B, the tested pH range was 4.5–6.5, and the temperature range was 25°C to 55°C. For the AnGH12 benchmark enzyme, the pH range was 5.5–7.5 and the temperature range was 40°C to 60°C. The substrate solutions were preheated for 10 minutes before the reaction, and the enzyme reactions were stopped by adding 0.1 M NaOH. Finally, the responses were determined from absorbance by the *p*-hydroxybenzoic acid hydrazide (PAHBAH) reducing sugar assay as described previously [48].

2.5. Determination of kinetic constants and thermal stability

Experiments to determine the kinetics constants were performed on citrus peel xyloglucan with 0.8 μM enzyme and a reaction time of 1–2 minutes. According to RSM results, the kinetics measurements took place in 50 mM acetate buffer at optimal pH and temperature conditions (Table 2). Five different substrate concentrations (1–15 g L^{-1}) were employed for all the enzymes. The steps, including preheating, termination of the enzyme reaction and the reducing sugar assay, were the same as in the RSM experiments. The results were defined as reducing sugar levels (μM glucose equivalents), and kinetic constants were determined by fitting the Michaelis-Menten equation to the data using non-linear regression in OriginPro 2021 (OriginLab, Northampton, MA, USA).

The thermal stability assays of the endoxyloglucanases were determined on citrus peel xyloglucan using the process described previously [49]. Briefly, the endoxyloglucanases were first incubated at different temperatures (40–70 °C) for up to 30 minutes. Then, thermal stability reactions took place in a substrate concentration of 40 g L^{-1} in 50 mM sodium acetate buffer. The reaction was performed at optimal pH (Table 2), and the enzyme dosage (E/S) was 0.05% (*w/w*). The temperature range for thermal stability test was 40–60 °C for PdGH12, 45–65 °C for PiGH12A, 50–65 °C for PiGH12B and 55–70 °C for AnGH12. The reducing sugar assay, substrate preheating and termination of the enzyme reaction were completed using the same procedure as described for the RSM experiment.

2.6. In silico sequence and structural analyses

The enzyme protein sequence alignment algorithm was created with Clustal Omega 1.2.4 using default settings. Six endoxyloglucanases, including the three new GH12 endoxyloglucanases from *Penicillium* spp., AnGH12 (benchmark enzyme), XEG (from *A. aculeatus*, Genbank: AAD02275.1) and BlGH12 (from *B. licheniformis*, Genbank: AAU42138.1) were selected to generate multiple protein sequence alignments and structural alignments. Homology models for all endoxyloglucanases, namely PdGH12, PiGH12A, PiGH12B and AnGH12, were predicted by the *Homology Modeling* building function in SWISS-MODEL [50], and XEG (PDB 3VL9) was selected as template for creating the homology model [51]. The alignment between the template (PDB 3VL9) and the homology model was performed by the *align* command in PyMOL (Version 1.1, Schrödinger, LLC, New York, NY, USA). By further structural alignment of both XEG (PDB number: 3VL9) and BlGH12 (PDB number: 2JEN) structures [33,51] to the homology models, the two xyloglucan ligands GXXG and XX, were introduced into the active site of the homology models for modelling the enzyme-xyloglucan complex. The distances between amino acids and the xyloglucan ligand were calculated automatically by using build-in *Zone* function of USCF Chimera [52].

Protein sequence identity was calculated using the command line version of BLAST+ for Protein-Protein BLAST 2.10.1+. By adding the "-use_sw_tback" flag, the Smith-Waterman algorithm was used to compute locally optimal alignments. The molecular weights of all endoxyloglucanases were calculated by enzyme protein sequence using the Sequence Manipulation Suite server (https://www.bioinformatics.org/sms2/protein_mw.html) [53]. Electrostatic plots for all enzymes were calculated by default settings on the APBS website (https://server.poissonboltzmann.org/), and the output files were visualized in USCF Chimera [52,54,55]. All structures were visualized with USCF Chimera [52].

2.7. Liquid chromatography-mass spectrometry (LC-MS) analysis

Two substrates, tamarind xyloglucan (1 g L^{-1}) and citrus peel xyloglucan (20 g L^{-1}), were hydrolyzed by the endoxyloglucanases at optimal pH and temperature conditions (Table 2) in 25 mM sodium acetate buffer. The reaction was carried out at E/S = 0.05% (*v/v*) for 24 hours. After enzymatic hydrolysis, the sample was heat-inactivated (95 °C for 10 minutes) and filtered on a 0.45 μm filter. Lastly, the sample was diluted to a 75% (*v/v*) final acetonitrile concentration for LC-MS analysis.

Analysis of reaction products were performed on an Ultimate3000RS UPLC from ThermoScientific (Sunnyvale, US) equipped with a TSKgel Amide-80, 2 μm column (2.0×150 mm) and 1 cm guard column of the same type, all from TOSOH (Greisheim, Germany). The column was operated at 55°C with a flow rate of 0.2 mL/min with a two-eluent system consisting of eluent A (0.1% formic acid in water) and eluent B (acetonitrile). Starting conditions were 75% B and hereafter; 0–5 min isocratic 75% B, 5–30 min linear gradient to 25% B, 30–33 min isocratic 25% B, directly back to starting conditions followed by 7 min re-equilibration (total run time of 40 min). The detector was an AmaZon SL iontrap mass spectrometer from Bruker Daltonics (Bremen, Germany) with ESI interface. The electrospray was operated in positive mode at 4.5 kV and 500 V end plate off set, 280 °C, nebulizer pressure of 3 bars and dry gas settings of 12 L min^{-1}. Target mass of 800 *m/z* and data acquisition was done with multiple reaction monitoring (MRM) settings of the ions (Table S5). Enzyme reaction products were observed primarily (but not exclusively) as double charged species as $[M+K+NH_4]^{2+}$. Data handling was performed in Bruker Compass DataAnalysis 5.2 and EICs (extracted ion chromatograms) were generated with fragmentation ions according to Table S5. Authenticated standards of XXXG, XXLG, XLLG and XXFG were included to verify product structure.

2.8. Statistics

Data are shown as mean ± standard deviation, and one-way ANOVA with Duncan's multiple range test was applied for comparing the value. P-values less than 0.05 ($p < 0.05$) is regarded as statistically significant. Statistical analyses were calculated using JMP pro 15.0 Statistical Software (SAS Institute, North Carolina, USA). All figures showing experiment results were created by OriginPro 2021 (OriginLab, Northampton, MA, USA).

3. Results and discussion

3.1. Bioinformatics-based subgrouping and analysis of family GH12 enzymes

The majority of the GH12 sequences are of fungal origin, mainly from Ascomycota, but also many from Basidiomycota (Fig. 1). The second largest superkingdom in GH12 is the Bacteria, of which most are Actinobacteria. The majority of the enzymes characterized in GH12 are endo-β-1,4-glucanases (EC 3.2.1.4) and they distribute across most of the GH family (Fig. 1). There is a cluster of endoxyloglucanases (EC 3.2.1.151) in the upper right corner. These are all fungal, mainly from Ascomycota and a few from Oomycota, and belong to CUPP groups GH12:6.1 and GH12:6.2. In addition, two bacterial ones: BlGH12 from *B. licheniformis* at the left side of the tree in GH12:5.1 and one from *S. fredii* in GH12:10.1, which is close to the branch of GH12:6.1 and GH12:6.2 (Fig. 1). Finally, AfCel12A from *A. fumigatus*, which has been assigned both endo-β-1,4-glucanase and endoxyloglucanase activity

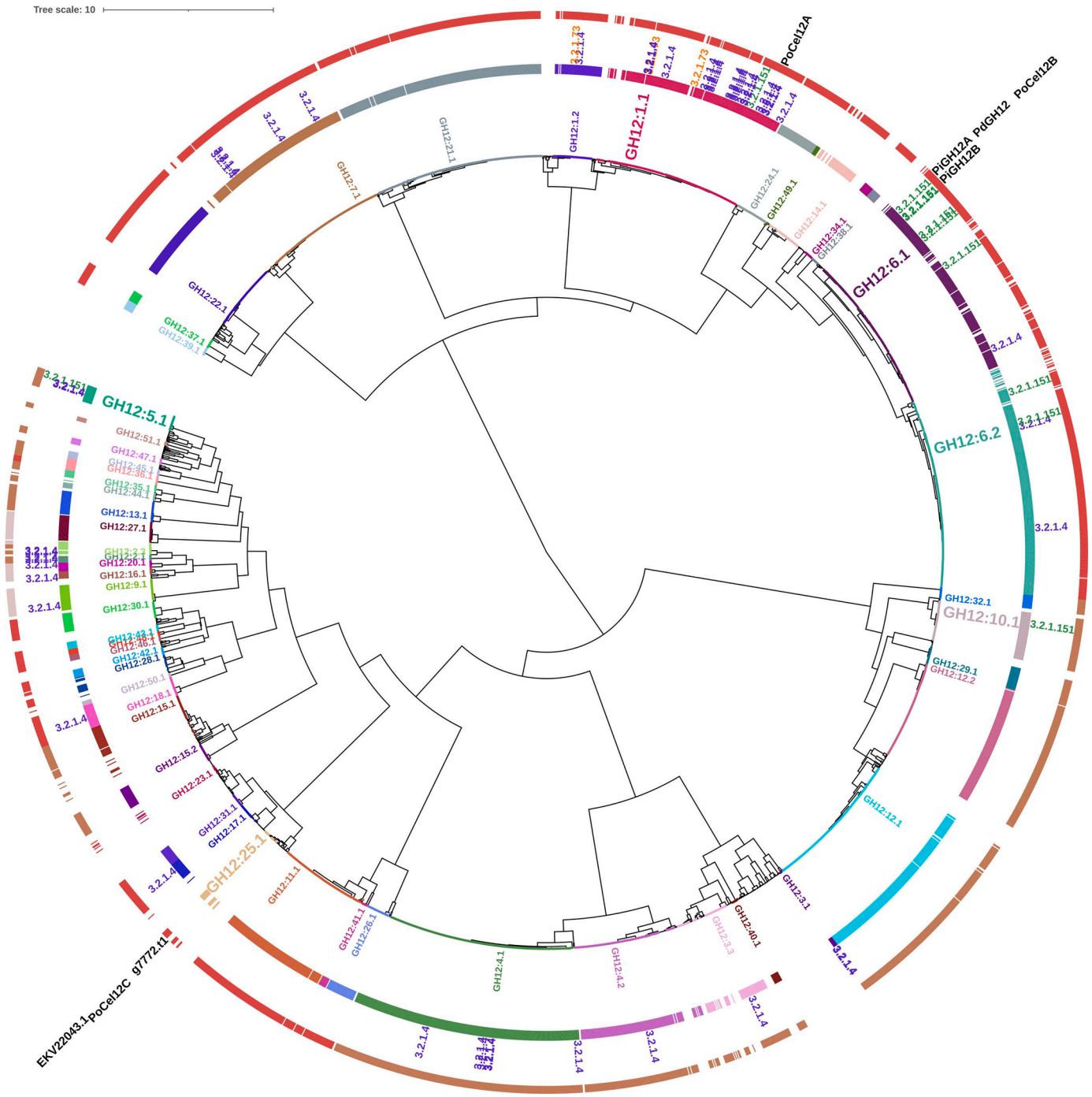

Fig. 1. CUPP dendrogram of GH12. CUPP groups (GH12:x.y) are indicated in the inner ring with accompanying label color. CUPP groups mentioned in the text are indicated in a bigger font. The middle ring indicates EC numbers of characterized members (data from the CAZy database): endo-β-1,4-glucanases (EC 3.2.1.4; blue), endoxyloglucanase (EC 3.2.1.151; green), and β-1,3-1,4-glucanase (EC 3.2.1.73; orange). The outer ring indicates superkingdom: Eukaryota (red), Bacteria (brown), and Archaea (grey). The online version of the tree, which includes indication of phyla, is available at https://itol.embl.de/tree/192381411146179170229587 8. GH12 enzymes from *Penicillium italicum*, *Penicillim digitatum* and *Penicillium oxalicum* are indicated with labels on the outer ring.

[19], is in GH12:1.1, a group that holds primarily endo-β-1,4-glucanases (EC 3.2.1.4) and two β-1,3–1,4-glucanase (EC 3.2.1.73). The subgrouping that has been suggested for GH12 enzymes from *Aspergillus* spp. [16] is also captured by the CUPP grouping: the members of subgroup I (endo-β-1,4-glucanases) are all in GH12:1.1, whereas the members of subgroup II (endoxyloglucanases) are in GH12:6.1 and GH12:6.2.

The association of *P. italicum* and *P. digitatum* with citrus fruits [35] directed our study to target these species in order to identify new enzymes active on citrus peel xyloglucan. Compared to other fungal species [56], *P. italicum* and *P. digitatum* have a relatively low number of degradative CAZymes (242 and 280, respectively; Table S1), which may reflect their narrow host range [35]. Based on the Augustus 2.5 prediction, three putative GH12 enzymes were identified in *P. italicum* GL-Gan1: g912.t1 (now PiGH12A) and g4763.t1 (now PiGH12B), which belong to CUPP group GH12:6.1 with the predicted function EC 3.2.1.151, and g7772.t1, which belongs to CUPP group GH12:25.1; this group has no characterized members, but the branch includes an endoglucanase (EC 3.2.1.4). No enzymes predicted to be of function EC 3.2.1.151 were found in any other GH families known to contain this activity. The two expressed GH12s from *P. italicum* GL-Gan1 have very high similarity (one amino acid difference) to KGO67155.1 and KGO76961.1 from *P. italicum* PHI-1. The two proteins from *P. italicum* PHI-1 are also present on cupp.info in the JGI genome (portal Penita1) with protein numbers 2250 and 4522 [57], and both belong to CUPP group GH12:6.1. *P. digitatum* Pd1 encodes for EKV19943.1 (now PdGH12), which belongs to GH12:6.1, EKV22043.1, which belongs to GH12:25.1, and EKV08566.1, whose prediction for GH12 had too low significance for proper assignment. Previously, three GH12 enzymes from *P. oxalicum* were found to display distinct substrate specificities [27] and these are captured by the CUPP grouping: PoCelB, which was highly specific for xyloglucan, is in GH12.6.1; PoCelA, which was most active on mixed-linkage β-glucan, is in GH12:1.1, whereas PoCelC, which had only low activity and no distinct substrate preference, is in GH12:25.1. So far, no examples of characterized GH12 endoxyloglucanases from the same CUPP group exists, but multigenicity has been described for other carbohydrate-degrading enzymes from filamentous fungi [49].

The sequence identity was high (84%) between PdGH12 and PiGH12A. In comparison, the sequence identity between two endoxyloglucanases from *P. italicum*, PiGH12A and PiGH12B, was only 70% (Table S3). The sequence identities between the *Penicillum* spp. endoxyloglucanases and the selected *Aspergillus* spp. endoxyloglucanases (the AnGH12 benchmark and XEG used for homology modelling) was in the 50–59% range, whereas the identity to previously characterized PoxXEG12A and PoCel12B from *P. oxalicum* [26,27], which differ by one amino acid to each other, was 58–60% (Table S3). The predicted molecular weight and signal peptide lengths of the three *Penicillium* spp. endoxyloglucanases were largely identical (Table 1). Similarly, the three endoxyloglucanases exhibited substantially identical enzyme properties with respect to CUPP group, predicted EC number and CUPP range (Table 1). This is in accordance with other fungal endoxyloglucanases from the same CUPP group, including PoxXEG12A from *P. oxalicum*, RmXEG12A and RmXEG12B from *R. miehei*, and XegA from *A. niveus* [21,26,29,37,38].

Several endoxyloglucanases from CUPP group GH12:6.1 and the neighbouring group GH12:6.2 have been identified as virulence factors in plant pathogens. These include FoEG1 from *Fusarium oxysporum* [58] and BcXYG1 from *Botrytis cinerea* [59] of GH12:6.1 like the *Penicillium* spp. endoxyloglucanases expressed in the current work, as well as XEG1 of *P. sojae* [30,60], VdEG1 and VdEG3 from *Verticillium dahlia* [61], which all belong to GH12:6.2 (Fig. 1). These endoxyloglucanases are upregulated during the early stages of plant infection and are responsible for infection of e.g. *Nicotiana benthamiana* [30,58,59]. They act as cell death-inducing pathogen-associated molecular patterns (PAMPs) in several plants including *N. benthamiana*, tobacco, tomato, and cotton [30,58,59]. Although this role is independent of enzyme activity [30,58,60], it was recently demonstrated that it is indeed the active site of XEG1 from *P. sojae*, which binds to the leucine-rich repeat (LRR) ectodomain of the receptor-like protein (RLP) of *N. benthamiana*, LRR-RLP RXEG1 [60], thereby eliciting a plant defense response to the pathogen invasion. Overexpression of *P. sojae* XEG1 elicited a response in *N. benthamiana* that limited the *P. sojae* infection [30], and addition of purified FoEG1 to plants increased their subsequent pathogen resistance [58]. Several different GH12s are also recognized by RXEG1 in *N. benthamiana* [62], indicating that this is a general role for the GH12 endoxyloglucanases of plant pathogen origin, especially considering that binding takes place in the active site, where amino acid residue conservation is high. Indeed, the active site residues shown to interact with *N. benthamiana* LRR-RKP RXEG1 [60], are conserved throughout the characterized and novel endoxyloglucanases of GH12:6.1 and GH12:6.2 (Fig. S1), indicating that all enzymes of these two CUPP groups – including the novel *Penicillium* spp. endoxyloglucanases – may play a similar role in their hosts. Although *P. italicum* and *P. digitatum* are postharvest pathogens [63,64], the observation that endoxyloglucanase activity is compensated by other GHs upon loss of the GH74 endoxyloglucanase in the preharvest pathogen *Xanthomonas citri* [65] supports the idea that GH12 endoxyloglucanases can play a role as virulence factors in citrus infection. Such roles in pathogenicity are not restricted to endoxyloglucanases, but have been observed for various cell wall-degrading enzymes [58].

3.2. Recombinant expression and reaction optimization of three *Penicillium*-derived GH12 endoxyloglucanases

PiGH12A, PiGH12B, PdGH12, and the benchmark enzyme AnGH12 were all successfully expressed in *P. pastoris* X-33 and purified to enable further characterization (Table 2, (Fig. S2). As predicted from sequence, their apparent size was 25–27 kDa as also observed for other fungal GH12 endoxyloglucanases [23,26–28]. Based on response surface methodology (RSM), the pH-temperature optima for hydrolysis of citrus peel xyloglucan were determined (Table 2): The enzymes PiGH12A and PiGH12B from *P. italicum* shared the pH optimum of 5.2–5.3, while the pH optimum for PdGH12 from *P. digitatum* had a slightly lower pH optimum at pH 4.6. All three enzymes from *Penicillum* spp. exhibited optimum reaction temperature for the 1 hour reaction around 35–37°C. Previously characterized GH12 endoxyloglucanases from *Penicillium* spp. have reported similar pH optima in the pH 4.6–5.0 range, and higher temperature optima of 50–60 °C albeit in a shorter reaction [27,28]. In comparison, AnGH12 from *A. nidulans* had a higher pH optimum at 6.1, and a higher optimum temperature of 48°C, although this was for a 30-minute reaction only (Table 2); this was in accordance with optimum conditions of pH 6.5 and 47°C previously observed on tamarind xyloglucan for the same enzyme [47].

Table 1
In silico prediction results for the new GH12s endoxyloglucanases.

Name	Amino Acids	Predicted Molecular Weight (kDa)	CUPP Group	CUPP Range	Predicted EC Number	Predicted Signal Peptide
PdGH12	252	27.52	GH12:6.1	127–238	EC 3.2.1.151	1–20
PiGH12A	252	27.60	GH12:6.1	127–238	EC 3.2.1.151	1–20
PiGH12B	246	26.62	GH12:6.1	121–233	EC 3.2.1.151	1–21

3.3. Enzyme kinetics and thermostability analysis of the selected *Penicillium*-derived GH12 endoxyloglucanases

The kinetic and thermal stability values for endoxyloglucanases were determined on citrus peel xyloglucan at the optimal reaction conditions (Table 2). The k_{cat} values of the two *P. italicum* endoxyloglucanases were similar, while that of PdGH12 was roughly twice as high. The K_M values ranged between 2.1 g L^{-1} for PiGH12A over 4.9 g L^{-1} for its orthologue PdGH12 to 6.6 g L^{-1} for PiGH12B (Table 3). The values are comparable with or slightly higher than those observed on tamarind xyloglucan for XGA from *P. canescens* (1.33 g L^{-1}), XG25 from *P. verruculosum* (0.28 g L^{-1}), and PoxXEG12A from *P. oxalicum* (3.12 g L^{-1}) using tamarind seed xyloglucan [26,28] (Table S4). AnGH12 showed a comparable K_M of 3.1 g L^{-1}, but a much lower k_{cat} value than the three *Penicillum*-derived enzymes (Table 3). Similar as well as lower K_M values have been obtained on tamarind xyloglucan for comparable enzymes from other *Aspergillus* spp., e.g. AaXeg12 from *A. aculeatus* (3.6 g L^{-1}), AclaXegA from *A. clavatus* (2.38 g L^{-1}), and AnXEG12A from *A. niger* (0.39 g L^{-1}) [15,17,20] (Table S4). The k_{cat}/K_M values were 71 and 86 L min^{-1} g^{-1} for PdGH12 and PiGH12A, respectively, whereas it was 4 times lower for PiGH12B, which had a k_{cat}/K_M comparable to that of AnGH12 (21–25 L min^{-1} g^{-1}; Table 3).

The thermal stability of the new endoxyloglucanases was assessed by measuring residual activity on citrus peel xyloglucan after incubation at 40–70 °C (Fig. S5, Table 4). All the *Penicillium* spp. endoxyloglucanases in our study showed excellent stability at 40 °C, thus emphasizing their stability at the optimal reaction temperature (35–37°C; Table 2). Nevertheless, they were sensitive to higher temperatures, and the half-lives were less than 16 min at 55 °C, with PiGH12B being the more thermostable among them (Table 4). In comparison, the *A. nidulans* AnGH12 was more thermostable (Table 4). This thermal stability was similar to the stability of AnXEG12A from *A. niger*, but higher than that of XEG from *A. aculeatus* [15,20].

3.4. Comparison of three selected *Penicillium*-derived GH12 endoxyloglucanases using structural models

In order to map the substrate binding sites and identify the putative catalytic residues of the three novel endoxyloglucanases, the protein sequence alignment between the three novel endoxyloglucanases, the benchmark AnGH12, and XEG and BlGH12, whose crystal structures contain relevant xyloglucan ligands in the negative and positive subsites, respectively [33,51], was analyzed (Fig. 2). From the sequence alignment, the two glutamic acid residues acting as catalytic nucleophile and catalytic acid/base, respectively, were identified. Similary, the Gly and Phe residues that facilitate substrate binding in the positive subsites and the Met that interacts with the O1 at the reducing end of the product

Table 2
Enzyme properties of the expressed endoxyloglucanases, including origin, apparent size (Fig. S2) and production yield (different letters means statistically significantly different, $p < 0.05$) and optimal reaction conditions (Fig. S3). The optimal reaction conditions were determined using citrus peel xyloglucan substrate in a reaction of 30 minutes (AnGH12) or 1 hour (PdGH12, PiGH12A and PiGH12B).

Name	Origin	Size on SDS-PAGE (kDa)	Expression Yield (mg/L)	pH Optimum	Temperature Optimum (°C)
PdGH12	*Penicillium digitatum*	~25	646 ± 13[b]	4.6	37
PiGH12A	*Penicillium italicum*	~26	541 ± 28[c]	5.2	37
PiGH12B	*Penicillium italicum*	~27	775 ± 30[a]	5.3	35
AnGH12	*Aspergillus nidulans*	~26	543 ± 20[c]	6.1	48

Table 3
Kinetic constants (Fig. S4) of the GH12 endoxyloglucanases on citrus peel xyloglucan at optimal conditions (Table 2). The V_{max} is calculated in μM reducing ends (glucose equivalents) released per minute, and the enzyme concentration of 0.8 μM was used in calculation of k_{cat}, which has the unit μM reducing ends (glucose equivalents) released per μM enzyme per minute.

Name	V_{max} (μM min^{-1})	K_M (g L^{-1})	k_{cat} (min^{-1})	k_{cat}/K_M (L min^{-1} g^{-1})
PdGH12	279	4.94	349	71
PiGH12A	146	2.12	183	86
PiGH12B	110	6.65	138	21
AnGH12	62.1	3.13	78	25

Table 4
Thermal stability (Fig. S5) of the GH12 endoxyloglucanases expressed as half-lives ($t_{½}$) in minutes at various temperatures. Remaining activity after incubation was determined on citrus peel xyloglucan at optimal conditions (Table 2).

Temperature (°C)	PdGH12	PiGH12A	PiGH12B	AnGH12
40	350	-	-	-
45	10	290	-	-
50	5.8	24	120	-
55	1.9	6.5	16	450
60	1.6	3.6	2.7	20
65	-	3.3	1.7	5.3
70	-	-	-	1.7

in BlGH12 from *B. licheniformis* (PDB 2JEN) [33], were conserved across all sequences. The two Trp and the Tyr that stack with the xyloglucan in the negative subsites of XEG from *A. aculeatus* (PDB 3VL9) [51] were conserved in all the fungal enzymes (Fig. 2). The alignment also emphasized several high-similarity regions between all six GH12 endoxyloglucanases, and notable differences between the five fungal enzymes and the bacterial BlGH12, which particularly included the substrate interacting residues identified in the negative subsites of BlGH12 (Fig. 2).

The XEG from *A. aculeatus* (PDB 3VL9) [51] was chosen by SWISS-MODEL [50] as the template structure to construct homology models of endoxyloglucanases; all homology models exhibited an RMSD value < 0.1 Å to the template and more than 50% of sequence identity (Table S3), indicating that the SWISS-MODEL prediction was reliable. Two xyloglucan ligands (GXXG and XX) from XEG (PDB 3VL9) and BlGH12 (PDB 2JEN), respectively, were included for making xyloglucan-xyloglucanase complex models covering both positive and negative subsites [33,51] (Fig. 3). The distances between the catalytic residues and the ligands were < 3 Å, indicating a reliably interpretable complex. The location of the catalytic residues and the binding sites were almost identical in the homology models, which showed a β-jelly roll fold characteristic of GH12 enzymes (Fig. 3 *Left*). The electrostatic plots indicated that surfaces of the orthologues PdGH12 and PiGH12A were less negatively charged than those of PiGH12B and AnGH12, which share higher sequence similarity with each other than with PiGH12A or PdGH12 (Fig. 3 *Middle*). All models present a negative charge in the negative subsites, yet the negative electrostatic potential appears higher in PiGH12B and AnGH12 (Fig. 3 *Middle*). As expected from the sequence alignment, the positions of the substrate-binding hydrophobic/aromatic residues Met, Trp, Tyr, and Phe were conserved in the active site pocket of all the endoxyloglucanase models with a single exception: PiGH12B has Tyr34 in place of the otherwise conserved Trp in subsite −4 (Fig. 3 *Right*). All of the characterized fungal GH12 endoxyloglucanases have a Trp in this position, except PiGH12B and AfCel12A from *A. fumigatus* [19], which have a Tyr, and FoEG1 and FGSG_05851 from *Fusarium* spp. [31,58], which have a Phe residue (Fig. S1). Future mutational studies could quantify the effect on enzyme kinetics of these differences in subsite −4 residues.

Xyloglucan exhibits a coiled conformation [66], which is also

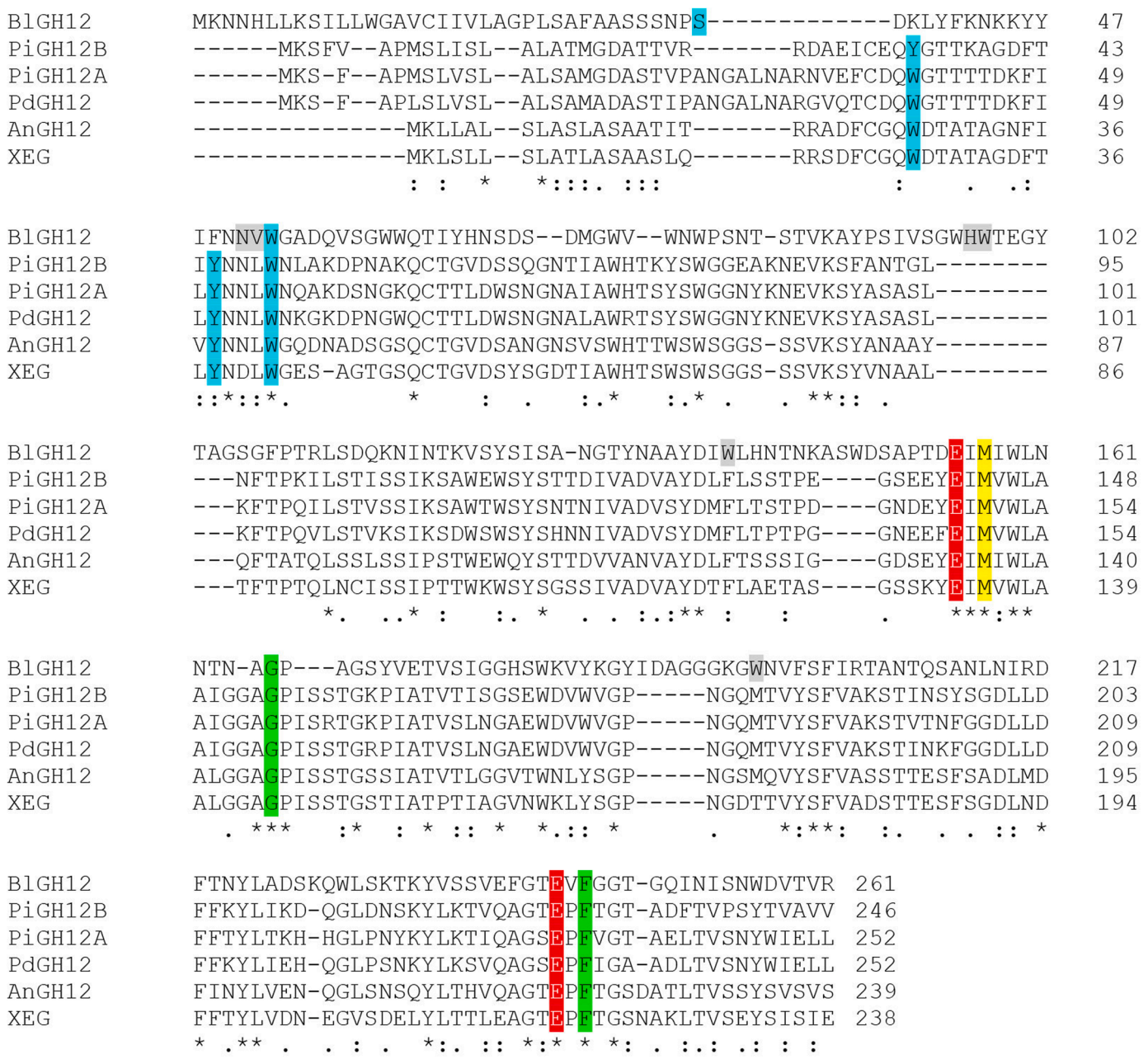

Fig. 2. Amino acid sequence alignment of endoxyloglucanases (PdGH12, PiGH12A, PiGH12B and AnGH12) with homology model template structure XEG from *Aspergillus aculeatus* (AAD02275.1) and BlGH12 from *Bacillus licheniformis* (AAU42138.1) included for xyloglucan ligand alignment (Fig. 3). The catalytic residues (red) are inferred from XEG and BlGH12. The interacting residues of the negative subsites identified in XEG [51] are indicated in cyan, whereas interacting residues of the positive subsites identified in BlGH12 [33] are indicated in green. The Met residue that interacts with the reducing end O1 of the hydrolysis product in BlGH12 [33] is marked in yellow. The N-terminal alignment is poor for the bacterial BlGH12, which has Ser36 (marked in cyan) aligned to Trp13 XEG (also cyan) when superimposing the two structures in PyMOL. Similarly, the interacting residues of the negative subsites in the bacterial BlGH12 (grey) [33] are not conserved with those of the fungal enzymes.

evident from the structure of the xyloglucan ligands superimposed on the homology models (Fig. 3 *Right*). Two Trp residues (Trp and Tyr in PiGH12B) interact with the glucose moieties in subsite −2 and −4, and have major impact on endoxyloglucanase activity [51]. Furthermore, a Tyr residue interacts with the xylose unit in subsite −3. Like all of these residues, the Met that interacts with the O1 at the reducing end of the product is also in place in all the homology models (Fig. 3 *Right*). Fewer interactions have been observed in the positive subsites, and only a single endoxyloglucanase structure with a positive subsite ligand exists [33]. For BlGH12, it was observed that the xylose unit in subsite +2 interacts with the backbone of Gly and stacks with Phe, whereas the xylose moiety in subsite +1 and the glucose moiety in subsite +2 made no interactions with the enzyme [33]; the homology models of the new fungal endoxyloglucanases apparently corroborate these observations (Fig. 3 *Right*).

3.5. Comparison of xyloglucan oligomer release from two xyloglucan substrates catalyzed by the Penicillum-derived GH12 endoxyloglucanases

The dominant hydrolysis products from tamarind xyloglucan (XXXG, XXLG, XLXG and XLLG, Fig. 4A) indicate that the endoxyloglucanases in our study have the same product and cleavage pattern as commonly

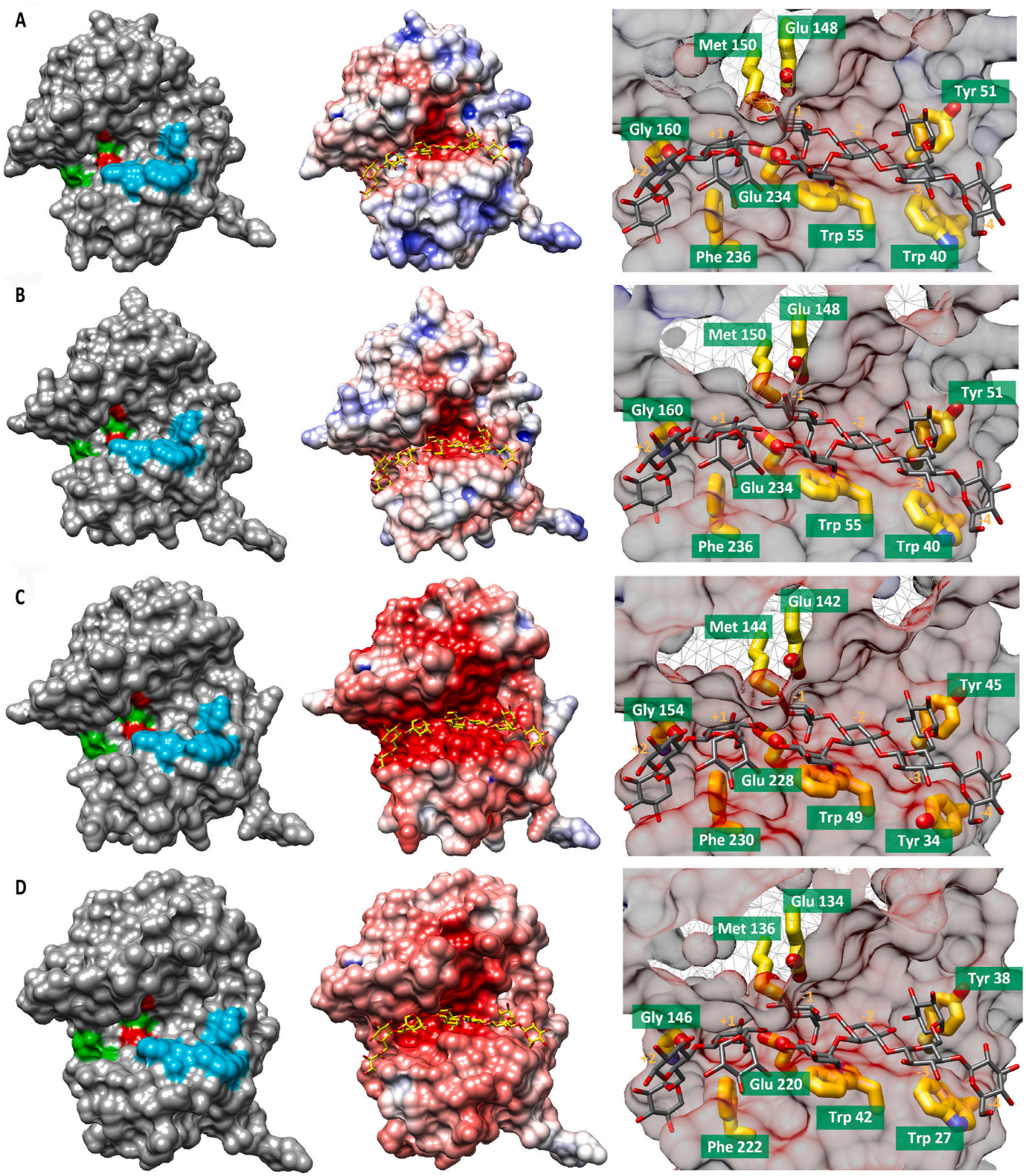

Fig. 3. Homology models of endoxyloglucanases generated by template (PDB 3VL9) alignment with SWISS-MODEL: A) PdGH12, B) PiGH12A, C) PiGH12B and D) AnGH12. *Left*: The surface structure of the endoxyloglucanases with predicted negative subsites −4 to −1 (cyan), catalytic Glu residues (red), product reducing end O1-interacting Met (green between the red), and positive subsites +1 and +2 (green to the left). The direction of the subsites (positive left, negative right) is reversed compared to the convention in order to improve the view into the active site. *Middle*: Electrostatic surface plots of the endoxyloglucanase-xyloglucan complexes, where red indicates negative electrostatic potential and blue positive electrostatic potential. *Right*: Magnification of the active site of the homology models of the endoxyloglucanase-xyloglucan complex. The xyloglucan ligands GXXG and XX were superimposed from the *Aspergillus aculeatus* XEG (PDB 3VL9) and *Bacillus licheniformis* BlGH12 (PDB 2JEN) structures, respectively, and these structures were also used for prediction of active site residues in the homology models.

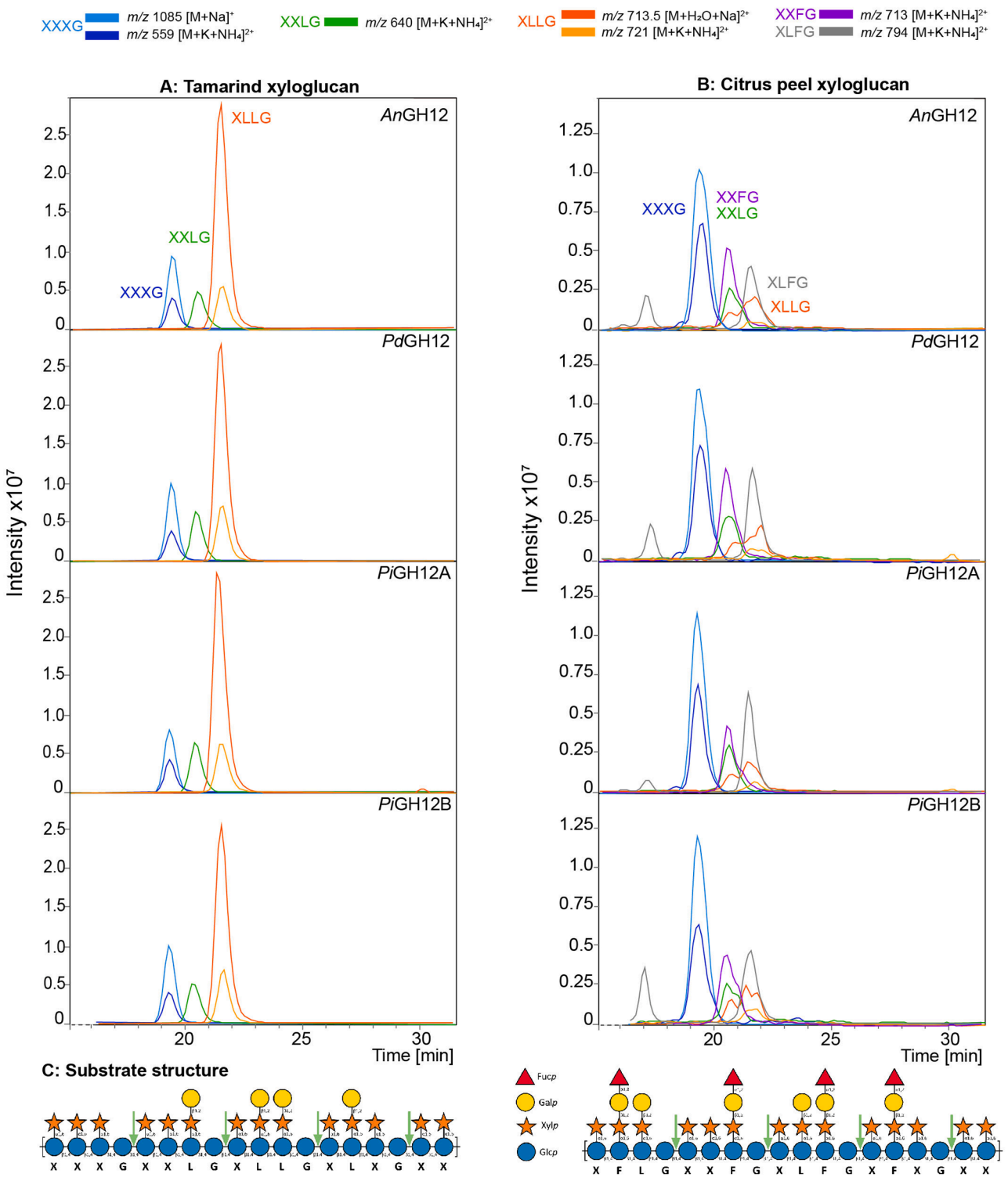

Fig. 4. LC-MS analysis of the endoxyloglucanase hydrolysis products obtained on A: tamarind xyloglucan and B: citrus peel xyloglucan. Within each panel the intensity is uniformly scaled and are therefore directly comparable. Chromatograms focus on the xyloglucan fragments from XXXG and larger. Please visit Fig. S6 for the entire chromatograms and Fig. S7 for MS spectra. Each type of xyloglucan fragment is defined by their peak and label color (XXXG blue; XXLG green; XLLG orange, XXFG purple; XLFG grey). The corresponding ion masses are given in Table S5. Note that several fragments occur as both single and double charged species (two color nuances distinguish the two species), and that the chromatographic resolution does not allow differentiation between structural isomers. The separation is primarily dictated by the degree of polymerization of the products (XXXG is DP7, XXLG is DP8, XLLG is DP9). Fucosylation decreases retention corresponding to one sugar unit in DP. The grey peak at a retention time of 17 min in panel B corresponds in *m/z* to XLFG, however does not match the fragmentation pattern of XLFG (data not shown) and should not be considered an XLFG fragment. More likely, this peak belongs to the monoisotopic pattern of XXG (Fig. S6). Panel C: Representative xyloglucan structures are given below the chromatograms; green arrows indicate endoxyloglucanase cleavage sites, and the reducing end stops at subsite +2 to mimic the homology models in Fig. 3.

observed for GH12 endoxyloglucanases, namely that they attack the xyloglucan backbone after unsubstituted glucosyl residues and do not fragment the product further [17,67]. This observation may be explained by the pocket-like shape of subsite −1 as compared to the otherwise very open active site cleft (Fig. 3). Tamarind xyloglucan does not contain significant amounts of fucosylations, whereas citrus peel xyloglucan does [2,12], and hence the hydrolysis products from citrus peel contain corresponding fucosylated fragments in addition to the products also observed from tamarind xyloglucan hydrolysis (i.e. XLFG/XFLG and XFXG/XXFG, Fig. 4B). Both tamarind xyloglucan and citrus peel xyloglucan have been extracted under alkaline conditions, hence all native acetylations [11] are expectedly removed, and no products with acetylations are observed. The analytical approach used here (HILIC-based chromatography) does not allow the differentiation between the products XLFG and XFLG or XFXG and XXFG, and therefore both structural isomers are possible. Besides the products presented in Fig. 4, a major product from citrus peel xyloglucan hydrolysis corresponds to an XXG fragment (Fig. S6). This relatively unusual product fragment is also present among reaction products from tamarind xyloglucan, however less prevalent compared to reactions on citrus peel xyloglucan. Whether this XXG fragment is a result of high enzyme loading (extensive degradation), or if the citrus peel xyloglucan contains short XXG stretches in the polymer is currently unknown. The latter could be an artificial modification of the native citrus peel xyloglucan caused by alkaline peeling during the extraction. Recently, it was suggested that a somewhat unusual distribution of xylosyl substitutions occur in apple xyloglucan [3].

Overall, the release of several xyloglucan fragments that carry both galactosyl and fucosyl side chains, and the magnitude of XXG release (Fig. S6) suggests extensive degradation of both tamarind and citrus peel xyloglucan by all the endoxyloglucanases. This observation is in accordance with previous reports that GH12 endoxyloglucanases generally tolerate various substitutions [68]. Quantification of hydrolysis yield is not trivial; authenticated standards are not readily available and the ionization and adduct pattern of the product oligosaccharides reveal high diversity in their propensity for acquiring charge and form adducts (Fig. 4). This is particularly evident from the two double charged species of XLLG (*m/z* 713 and *m/z* 721). Even at dilute conditions, several adducts and charge states appear (data not shown), leading to risk of severe under- or overestimation in cases where quantification is performed relative to a single species (e.g. XXXG). We therefore refrain from exact product quantification. Nevertheless, it is evident from the chromatograms (Fig. 4) that XLLG is the major product from tamarind hydrolysis, whereas XXXG is the major product from citrus peel xyloglucan, indicating longer stretches of X-rich backbone in the latter.

4. Conclusion

This study reports the expression of three active GH12 enzymes from two *Penicillium* spp. that are known to be citrus pathogens and their characterization on citrus peel xyloglucan. The functional subdivision of GH12 performed by CUPP facilitated the identification of xyloglucan-active enzymes in the family. Although activity on linear β-glucan cannot be ruled out for these *Penicillium*-derived enzymes based on the current work, their close relationship with other highly xyloglucan-specific endoglucanases [16,27,28] makes a preference for xyloglucan likely (Fig. 1). All three enzymes released xyloglucan oligosaccharides from tamarind xyloglucan and from fucosylated citrus peel xyloglucan. The enzyme action and xyloglucan products reflected the substitution diversity between these two substrates. The substitution of a conserved Trp with a Tyr residue in subsite −4 of PiGH12B did not alter the product release pattern. Enzymatically released xyloglucan oligosaccharides can exert beneficial health effects. Fucosylated xyloglucan oligosaccharides, which are abundant in citrus peel waste, may also serve as donor substrates in the synthesis of fucosylated human milk oligosaccharides.

CRediT authorship contribution statement

Kristian Barrett: Supervision, Software, Investigation, Formal analysis. **Kai Li:** Writing – original draft, Visualization, Methodology, Investigation, Funding acquisition, Formal analysis. **Anne S. Meyer:** Writing – review & editing, Supervision, Resources, Project administration, Methodology, Funding acquisition, Conceptualization. **Jane W. Agger:** Writing – review & editing, Writing – original draft, Visualization, Resources, Investigation, Formal analysis. **Birgitte Zeuner:** Writing – review & editing, Writing – original draft, Visualization, Supervision, Investigation.

Declaration of Competing Interest

The authors declare no competing interest.

Data Availability

Data will be made available on request.

Acknowledgments

This study was support by a grant from the Chinese Scholarship Council (CSC) to Kai Li.

Appendix A. Supporting information

Supplementary data associated with this article can be found in the online version at doi:10.1016/j.enzmictec.2024.110441.

References

[1] FAO, Citrus Fruit Statistical Compendium 2020, Rome, 2021.
[2] T.L. Biel-Nielsen, K. Li, S.O. Sørensen, J.J.P. Sejberg, A.S. Meyer, J. Holck, Utilization of industrial citrus pectin side streams for enzymatic production of human milk oligosaccharides, Carbohydr. Res 519 (2022), https://doi.org/10.1016/j.carres.2022.108627.
[3] M. Chen, J. Mac-Béar, D. Ropartz, M. Lahaye, Biorefinery of apple pomace: new insights into xyloglucan building blocks, Carbohydr. Polym. 290 (2022), https://doi.org/10.1016/j.carbpol.2022.119526.
[4] A.T. Hotchkiss, J.A. Renye, A.K. White, A. Nunez, G.K.P. Guron, H. Chau, S. Simon, C. Poveda, G. Walton, R. Rastall, C. Khoo, Cranberry Arabino-Xyloglucan and Pectic Oligosaccharides Induce *Lactobacillus* Growth and Short-Chain Fatty Acid Production, Microorganisms 10 (2022), https://doi.org/10.3390/microorganisms10071346.
[5] H. Chen, X. Jiang, S. Li, W. Qin, Z. Huang, Y. Luo, H. Li, D. Wu, Q. Zhang, Y. Zhao, B. Yu, C. Li, D. Chen, Possible beneficial effects of xyloglucan from its degradation by gut microbiota, Trends Food Sci. Technol. 97 (2020) 65–75, https://doi.org/10.1016/j.tifs.2020.01.001.
[6] C.H. Zhu, Y.X. Li, Y.C. Xu, N.N. Wang, Q.J. Yan, Z.Q. Jiang, Tamarind Xyloglucan Oligosaccharides Attenuate Metabolic Disorders via the Gut–Liver Axis in Mice with High-Fat-Diet-Induced Obesity, Foods 12 (2023), https://doi.org/10.3390/foods12071382.
[7] B. Zeuner, J. Muschiol, J. Holck, M. Lezyk, M.R. Gedde, C. Jers, J.D. Mikkelsen, A. S. Meyer, Substrate specificity and transfucosylation activity of GH29 α-L-fucosidases for enzymatic production of human milk oligosaccharides, N. Biotechnol. 41 (2018) 34–45, https://doi.org/10.1016/j.nbt.2017.12.002.
[8] M. Lezyk, C. Jers, L. Kjaerulff, C.H. Gotfredsen, M.D. Mikkelsen, J.D. Mikkelsen, Novel α-L-fucosidases from a soil metagenome for production of fucosylated human milk oligosaccharides, PLoS One 11 (2016) e0147438, https://doi.org/10.1371/journal.pone.0147438.
[9] S.C. Fry, The Structure and Functions of Xyloglucan, J. Exp. Bot. 40 (1989) 1–11, https://doi.org/10.1093/jxb/40.1.1.
[10] M. Pauly, Q. Qin, H. Greene, P. Albersheim, A. Darvill, W.S. York, Changes in the structure of xyloglucan during cell elongation, Planta 212 (2001) 842–850, https://doi.org/10.1007/s004250000448.
[11] A. Schultink, L. Liu, L. Zhu, M. Pauly, Structural diversity and function of xyloglucan sidechain substituents, Plants 3 (2014) 526–542, https://doi.org/10.3390/plants3040526.
[12] B. Zeuner, M. Vuillemin, J. Holck, J. Muschiol, A.S. Meyer, Improved Transglycosylation by a Xyloglucan-Active α-l-Fucosidase from *Fusarium graminearum*, J. Fungi 6 (2020) 295, https://doi.org/10.3390/jof6040295.
[13] E. Drula, M. Garron, S. Dogan, V. Lombard, B. Henrissat, N. Terrapon, The carbohydrate-active enzyme database: functions and literature, Nucleic Acids Res (2021) 1–7, https://doi.org/10.1093/nar/gkab1045.

[14] R. Rashmi, K.R. Siddalingamurthy, Microbial xyloglucanases: a comprehensive review, Biocatal. Biotransformation 36 (2018) 280–295, https://doi.org/10.1080/10242422.2017.1417394.

[15] M. Pauly, L.N. Andersen, S. Kauppinen, L.V. Kofod, W.S. York, P. Albersheim, A. Darvill, A xyloglucan-specific endo-beta-1,4-glucanase from *Aspergillus aculeatus*: expression cloning in yeast, purification and characterization of the recombinant enzyme, Glycobiology 9 (1999), https://doi.org/10.1093/glycob/9.1.93.

[16] S.V. Rykov, P. Kornberger, J. Herlet, N.V. Tsurin, I.N. Zorov, V.V. Zverlov, W. Liebl, W.H. Schwarz, S.V. Yarotsky, O.V. Berezina, Novel endo-(1,4)-β-glucanase Bgh12A and xyloglucanase Xgh12B from *Aspergillus cervinus* belong to GH12 subgroup I and II, respectively, Appl. Microbiol Biotechnol. 103 (2019) 7553–7566, https://doi.org/10.1007/s00253-019-10006-x.

[17] A.R.L. Damásio, M.V. Rubio, L.C. Oliveira, F. Segato, B.A. Dias, A.P. Citadini, D. A. Paixão, F.M. Squina, Understanding the function of conserved variations in the catalytic loops of fungal glycoside hydrolase family 12, Biotechnol. Bioeng. 111 (2014), https://doi.org/10.1002/bit.25209.

[18] J.W. Agger, T. Isaksen, A. Várnai, S. Vidal-Melgosa, W.G.T. Willats, R. Ludwig, S. J. Horn, V.G.H. Eijsink, B. Westereng, Discovery of LPMO activity on hemicelluloses shows the importance of oxidative processes in plant cell wall degradation, Proc. Natl. Acad. Sci. USA 111 (2014), https://doi.org/10.1073/pnas.1323629111.

[19] E. Vlasenko, M. Schülein, J. Cherry, F. Xu, Substrate specificity of family 5, 6, 7, 9, 12, and 45 endoglucanases, Bioresour. Technol. 101 (2010) 2405–2411, https://doi.org/10.1016/j.biortech.2009.11.057.

[20] E.R. Master, Y. Zheng, R. Storms, A. Tsang, J. Powlowski, A xyloglucan-specific family 12 glycosyl hydrolase from *Aspergillus niger*: recombinant expression, purification and characterization, Biochem J. 411 (2008), https://doi.org/10.1042/BJ20070819.

[21] A.R.L. Damásio, L.F.C. Ribeiro, L.F. Ribeiro, G.P. Furtado, F. Segato, F.B. R. Almeida, A.C. Crivellari, M.S. Buckeridge, T.A.C.B. Souza, M.T. Murakami, R. J. Ward, R.A. Prade, M.L.T.M. Polizeli, Functional characterization and oligomerization of a recombinant xyloglucan-specific endo-β-1,4-glucanase (GH12) from *Aspergillus niveus*, Biochim Biophys. Acta Proteins Prote 1824 (2012) 461–467, https://doi.org/10.1016/j.bbapap.2011.12.005.

[22] S. Bauer, P. Vasu, S. Persson, A.J. Mort, C.R. Somerville, Development and application of a suite of polysaccharide-degrading enzymes for analyzing plant cell walls, Proc. Natl. Acad. Sci. 103 (2006) 11417–11422, https://doi.org/10.1073/pnas.0604632103.

[23] T. Matsuzawa, A. Kameyama, Y. Nakamichi, K. Yaoi, Identification and characterization of two xyloglucan-specific endo-1,4-glucanases in *Aspergillus oryzae*, Appl. Microbiol Biotechnol. 104 (2020), https://doi.org/10.1007/s00253-020-10883-7.

[24] G.L. Vitcosque, L.F.C. Ribeiro, R.C. de Lucas, T.M. da Silva, L.F. Ribeiro, A.R. de Lima Damasio, C.S. Farinas, A.Z.L. Gonçalves, F. Segato, M.S. Buckeridge, J. A. Jorge, M. de, L.T.M. Polizeli, The functional properties of a xyloglucanase (GH12) of *Aspergillus terreus* expressed in *Aspergillus nidulans* may increase performance of biomass degradation, Appl. Microbiol Biotechnol. 100 (2016), https://doi.org/10.1007/s00253-016-7589-2.

[25] T. Matsuzawa, A. Watanabe, T. Shintani, K. Gomi, K. Yaoi, Enzymatic degradation of xyloglucans by *Aspergillus* species: a comparative view of this genus, Appl. Microbiol Biotechnol. 105 (2021) 2701–2711, https://doi.org/10.1007/s00253-021-11236-8.

[26] L. Xian, F. Wang, X. Yin, J.-X. Feng, Identification and characterization of an acidic and acid-stable endoxyloglucanase from *Penicillium oxalicum*, Int J. Biol. Macromol. 86 (2016), https://doi.org/10.1016/j.ijbiomac.2016.01.105.

[27] Z. Zhu, J. Qu, L. Yu, X. Jiang, G. Liu, L. Wang, Y. Qu, Y. Qin, Three glycoside hydrolase family 12 enzymes display diversity in substrate specificities and synergistic action between each other, Mol. Biol. Rep. 46 (2019) 5443–5454, https://doi.org/10.1007/s11033-019-04999-x.

[28] O.A. Sinitsyna, E.A. Fedorova, A.G. Pravilnikov, A.M. Rozhkova, A. A. Skomarovsky, V.Y. Matys, T.M. Bubnova, O.N. Okunev, Y.P. Vinetsky, A. P. Sinitsyn, Isolation and properties of xyloglucanases of *Penicillium* sp, Biochem. (Mosc.) 75 (2010) 41–49, https://doi.org/10.1134/S0006297910010062.

[29] S. Song, Y. Tang, S. Yang, Q. Yan, P. Zhou, Z. Jiang, Characterization of two novel family 12 xyloglucanases from the thermophilic *Rhizomucor miehei*, Appl. Microbiol Biotechnol. 97 (2013), https://doi.org/10.1007/s00253-013-4770-8.

[30] Z. Ma, T. Song, L. Zhu, W. Ye, Y. Wang, Y. Shao, S. Dong, Z. Zhang, D. Dou, X. Zheng, B.M. Tyler, Y. Wang, A *Phytophthora sojae* glycoside hydrolase 12 protein is a major virulence factor during soybean infection and is recognized as a PAMP, Plant Cell 27 (2015) 2057–2072, https://doi.org/10.1105/tpc.15.00390.

[31] O. Habrylo, X. Song, A. Forster, J.-M. Jeltsch, V. Phalip, Characterization of the four GH12 Endoxylanases from the plant pathogen *Fusarium graminearum*, J. Microbiol Biotechnol. 22 (2012), https://doi.org/10.4014/jmb.1112.11019.

[32] T. Takeda, M. Takahashi, T. Nakanishi-Masuno, Y. Nakano, H. Saitoh, A. Hirabuchi, S. Fujisawa, R. Terauchi, Characterization of endo-1,3-1,4-β-glucanases in GH family 12 from *Magnaporthe oryzae*, Appl. Microbiol Biotechnol. 88 (2010), https://doi.org/10.1007/s00253-010-2781-2.

[33] T.M. Gloster, F.M. Ibatullin, K. Macauley, J.M. Eklöf, S. Roberts, J.P. Turkenburg, M.E. Bjørnvad, P.L. Jørgensen, S. Danielsen, K.S. Johansen, T.V. Borchert, K. S. Wilson, H. Brumer, G.J. Davies, Characterization and three-dimensional structures of two distinct bacterial xyloglucanases from families GH5 and GH12, J. Biol. Chem. 282 (2007), https://doi.org/10.1074/jbc.M700224200.

[34] J. Dorival, S. Philys, E. Giuntini, R. Brailly, J. de Ruyck, M. Czjzek, E. Biondi, C. Bompard, Structural and enzymatic characterisation of the Type III effector NopAA (=GunA) from *Sinorhizobium fredii* USDA257 reveals a Xyloglucan hydrolase activity, Sci. Rep. 10 (2020), https://doi.org/10.1038/s41598-020-67069-4.

[35] K. Barrett, K. Jensen, A.S. Meyer, J.C. Frisvad, L. Lange, Fungal secretome profile categorization of CAZymes by function and family corresponds to fungal phylogeny and taxonomy: Example *Aspergillus* and *Penicillium*, Sci. Rep. 10 (2020), https://doi.org/10.1038/s41598-020-61907-1.

[36] K. Barrett, H. Zhao, P. Hao, A. Bacic, L. Lange, J. Holck, A.S. Meyer, Discovery of novel secretome CAZymes from *Penicillium sclerotigenum* by bioinformatics and explorative proteomics analyses during sweet potato pectin digestion, Front Bioeng. Biotechnol. 10 (2022), https://doi.org/10.3389/fbioe.2022.950259.

[37] K. Barrett, C.J. Hunt, L. Lange, A.S. Meyer, Conserved unique peptide patterns (CUPP) online platform: peptide-based functional annotation of carbohydrate active enzymes, Nucleic Acids Res 48 (2020) 110–115, https://doi.org/10.1093/nar/gkaa375.

[38] K. Barrett, L. Lange, Peptide-based functional annotation of carbohydrate-active enzymes by conserved unique peptide patterns (CUPP), Biotechnol. Biofuels 12 (2019) 102, https://doi.org/10.1186/s13068-019-1436-5.

[39] J. Qiu, K. Barrett, C. Wilkens, A.S. Meyer, Bioinformatics based discovery of new keratinases in protease family M36, N. Biotechnol. 68 (2022) 19–27, https://doi.org/10.1016/j.nbt.2022.01.004.

[40] V.N. Perna, K. Barrett, A.S. Meyer, B. Zeuner, Substrate specificity and transglycosylation capacity of α-L-fucosidases across GH29 assessed by bioinformatics-assisted selection of functional diversity, Glycobiology (2023), https://doi.org/10.1093/glycob/cwad029.

[41] T. Feng, K.P. Yan, M.D. Mikkelsen, A.S. Meyer, H.A. Schols, B. Westereng, J. D. Mikkelsen, Characterisation of a novel endo-xyloglucanase (XcXGHA) from *Xanthomonas* that accommodates a xylosyl-substituted glucose at subsite −1, Appl. Microbiol Biotechnol. 98 (2014) 9667–9679, https://doi.org/10.1007/s00253-014-5825-1.

[42] O. Keller, M. Kollmar, M. Stanke, S. Waack, A novel hybrid gene prediction method employing protein multiple sequence alignments, Bioinformatics 27 (2011) 757–763, https://doi.org/10.1093/bioinformatics/btr010.

[43] I. Letunic, P. Bork, Interactive tree of life (iTOL) v5: An online tool for phylogenetic tree display and annotation, Nucleic Acids Res 49 (2021) W293–W296, https://doi.org/10.1093/nar/gkab301.

[44] J.J. Almagro Armenteros, K.D. Tsirigos, C.K. Sønderby, T.N. Petersen, O. Winther, S. Brunak, G. von Heijne, H. Nielsen, SignalP 5.0 improves signal peptide predictions using deep neural networks, Nat. Biotechnol. 37 (2019) 420–423, https://doi.org/10.1038/s41587-019-0036-z.

[45] M. Michalak, L.V. Thomassen, H. Roytio, A.C. Ouwehand, A.S. Meyer, J. D. Mikkelsen, Expression and characterization of an endo-1,4-β-galactanase from *Emericella nidulans* in *Pichia pastoris* for enzymatic design of potentially prebiotic oligosaccharides from potato galactans, Enzym. Micro Technol. 50 (2012) 121–129, https://doi.org/10.1016/j.enzmictec.2011.11.001.

[46] M. Vuillemin, J. Holck, M. Matwiejuk, E.S. Moreno Prieto, J. Muschiol, D. Molnar-Gabor, A.S. Meyer, B. Zeuner, Improvement of the Transglycosylation Efficiency of a Lacto-*N*-Biosidase from *Bifidobacterium bifidum* by Protein Engineering, Appl. Sci. 11 (2021) 11493, https://doi.org/10.3390/app112311493.

[47] S. Bauer, P. Vasu, S. Persson, A.J. Mort, C.R. Somerville, Development and application of a suite of polysaccharide-degrading enzymes for analyzing plant cell walls, Proc. Natl. Acad. Sci. USA 103 (2006) 11417–11422, https://doi.org/10.1073/pnas.0604632103.

[48] M. Lever, A new reaction for colorimetric determination of carbohydrates, Anal. Biochem 47 (1972) 273–279, https://doi.org/10.1016/0003-2697(72)90301-6.

[49] B. Zeuner, T.B. Thomsen, M.A. Stringer, K.B.R.M. Krogh, A.S. Meyer, J. Holck, A. S. Meyer, Comparative Characterization of *Aspergillus* Pectin Lyases by Discriminative Substrate Degradation Profiling, Front Bioeng. Biotechnol. 8 (2020) 873, https://doi.org/10.3389/fbioe.2020.00873.

[50] A. Waterhouse, M. Bertoni, S. Bienert, G. Studer, G. Tauriello, R. Gumienny, F. T. Heer, T.A.P. de Beer, C. Rempfer, L. Bordoli, R. Lepore, T. Schwede, SWISS-MODEL: homology modelling of protein structures and complexes, Nucleic Acids Res 46 (2018) W296–W303, https://doi.org/10.1093/nar/gky427.

[51] T. Yoshizawa, T. Shimizu, H. Hirano, M. Sato, H. Hashimoto, Structural Basis for Inhibition of Xyloglucan-specific Endo-β-1,4-glucanase (XEG) by XEG-Protein Inhibitor, J. Biol. Chem. 287 (2012) 18710–18716, https://doi.org/10.1074/jbc.M112.350520.

[52] E.F. Pettersen, T.D. Goddard, C.C. Huang, G.S. Couch, D.M. Greenblatt, E.C. Meng, T.E. Ferrin, U.C.S.F. Chimera?, A visualization system for exploratory research and analysis, J. Comput. Chem. 25 (2004) 1605–1612, https://doi.org/10.1002/jcc.20084.

[53] P. Stothard, The Sequence Manipulation Suite: JavaScript Programs for Analyzing and Formatting Protein and DNA Sequences, Biotechniques 28 (2000) 1102–1104, https://doi.org/10.2144/00286ir01.

[54] T.J. Dolinsky, J.E. Nielsen, J.A. McCammon, N.A. Baker, PDB2PQR: an automated pipeline for the setup of Poisson-Boltzmann electrostatics calculations, Nucleic Acids Res 32 (2004) W665–W667, https://doi.org/10.1093/nar/gkh381.

[55] N.A. Baker, D. Sept, S. Joseph, M.J. Holst, J.A. McCammon, Electrostatics of nanosystems: Application to microtubules and the ribosome, Proc. Natl. Acad. Sci. USA 98 (2001) 10037–10041, https://doi.org/10.1073/pnas.181342398.

[56] L. Lange, K. Barrett, A.S. Meyer, New method for identifying fungal kingdom enzyme hotspots from genome sequences, J. Fungi 7 (2021), https://doi.org/10.3390/jof7030207.

[57] K. Barrett, C.J. Hunt, L. Lange, I.V. Grigoriev, A.S. Meyer, Conserved unique peptide patterns (CUPP) online platform 2.0: Implementation of +1000 JGI fungal genomes, Nucleic Acids Res 51 (2023) W108–W114, https://doi.org/10.1093/nar/gkad385.

[58] L. Zhang, J. Yan, Z. Fu, W. Shi, V. Ninkuu, G. Li, X. Yang, H. Zeng, FoEG1, a secreted glycoside hydrolase family 12 protein from *Fusarium oxysporum*, triggers cell death and modulates plant immunity, Mol. Plant Pathol. 22 (2021) 522–538, https://doi.org/10.1111/mpp.13041.

[59] W. Zhu, M. Ronen, Y. Gur, A. Minz-Dub, G. Masrati, N. Ben-Tal, A. Savidor, I. Sharon, E. Eizner, O. Valerius, G.H. Braus, K. Bowler, M. Bar-Peled, A. Sharon, BcXYG1, a secreted xyloglucanase from *Botrytis cinerea*, triggers both cell death and plant immune responses, Plant Physiol. 175 (2017) 438–456, https://doi.org/10.1104/pp.17.00375.

[60] Y. Sun, Y. Wang, X. Zhang, Z. Chen, Y. Xia, L. Wang, Y. Sun, M. Zhang, Y. Xiao, Z. Han, Y. Wang, J. Chai, Plant receptor-like protein activation by a microbial glycoside hydrolase, Nature 610 (2022) 335–342, https://doi.org/10.1038/s41586-022-05214-x.

[61] Y.J. Gui, J.Y. Chen, D.D. Zhang, N.Y. Li, T.G. Li, W.Q. Zhang, X.Y. Wang, D.P. G. Short, L. Li, W. Guo, Z.Q. Kong, Y.M. Bao, K.V. Subbarao, X.F. Dai, *Verticillium dahliae* manipulates plant immunity by glycoside hydrolase 12 proteins in conjunction with carbohydrate-binding module 1, Environ. Microbiol 19 (2017) 1914–1932, https://doi.org/10.1111/1462-2920.13695.

[62] Y. Wang, Y. Xu, Y. Sun, H. Wang, J. Qi, B. Wan, W. Ye, Y. Lin, Y. Shao, S. Dong, B. M. Tyler, Y. Wang, Leucine-rich repeat receptor-like gene screen reveals that *Nicotiana* RXEG1 regulates glycoside hydrolase 12 MAMP detection, Nat. Commun. 9 (2018), https://doi.org/10.1038/s41467-018-03010-8.

[63] A.M. Kanashiro, D.Y. Akiyama, K.C. Kupper, T.P. Fill, *Penicillium italicum*: An Underexplored Postharvest Pathogen, Front Microbiol 11 (2020), https://doi.org/10.3389/fmicb.2020.606852.

[64] J.H. Costa, J.M. Bazioli, J.G. de Moraes Pontes, T.P. Fill, *Penicillium digitatum* infection mechanisms in citrus: What do we know so far? Fungal Biol. 123 (2019) 584–593, https://doi.org/10.1016/j.funbio.2019.05.004.

[65] P.S. Vieira, I.M. Bonfim, E.A. Araujo, R.R. Melo, A.R. Lima, M.R. Fessel, D.A. A. Paixão, G.F. Persinoti, S.A. Rocco, T.B. Lima, R.A.S. Pirolla, M.A.B. Morais, J.B. L. Correa, L.M. Zanphorlin, J.A. Diogo, E.A. Lima, A. Grandis, M.S. Buckeridge, F. C. Gozzo, C.E. Benedetti, I. Polikarpov, P.O. Giuseppe, M.T. Murakami, Xyloglucan processing machinery in *Xanthomonas* pathogens and its role in the transcriptional activation of virulence factors, Nat. Commun. 12 (2021), https://doi.org/10.1038/s41467-021-24277-4.

[66] Y. Zheng, X. Wang, Y. Chen, E. Wagner, D.J. Cosgrove, Xyloglucan in the primary cell wall: assessment by selective enzyme digestions and nanogold affinity tags, Plant J. 93 (2018) 211–226, https://doi.org/10.1111/tpj.13778.

[67] H.J. Gilbert, H. Stålbrand, H. Brumer, How the walls come crumbling down: recent structural biochemistry of plant polysaccharide degradation, Curr. Opin. Plant Biol. 11 (2008) 338–348, https://doi.org/10.1016/j.pbi.2008.03.004.

[68] H.J. Gilbert, The biochemistry and structural biology of plant cell wall deconstruction, Plant Physiol. 153 (2010) 444–455, https://doi.org/10.1104/pp.110.156646.